



CrossMark  
click for updates

Cite this: *RSC Adv.*, 2015, 5, 29828

# Spiro[fluorene-9,9'-xanthene]-based universal hosts for understanding structure–property relationships in RGB and white PhOLEDs†

Yan Qian,<sup>‡a</sup> Yeren Ni,<sup>‡a</sup> Shouzhen Yue,<sup>‡b</sup> Wenwen Li,<sup>a</sup> Shufen Chen,<sup>a</sup> Zhensong Zhang,<sup>b</sup> Linghai Xie,<sup>\*a</sup> Mingli Sun,<sup>a</sup> Yi Zhao<sup>\*b</sup> and Wei Huang<sup>\*ac</sup>

Ingenious construction of state-of-the-art models of electrophosphorescent hosts for uncovering the deep role of different molecular modifications in PhOLEDs performances is crucial for rational cumulative improvements of device efficiency and for accelerating their commercialization. A series of conjugation-interrupted spiro[fluorene-9,9'-xanthene](SFX)/9-arylfuorenes (AFs) hybrid host materials have been designed and synthesized by concise two-step reactions, and have been demonstrated to serve as universal hosts for low voltage blue, green, red and single-emitting layer white PhOLEDs. By varying the electronegativity and position of the bulky AF substitutes, two independent, selective methods for fine tuning frontier molecular orbital energy levels without affecting the high triplet energy level ( $T_1$ ) have been realized. This offers either facilitated hole- or electron-injection/blocking without influencing the optical properties, which can explain the performance of the corresponding RGB PhOLEDs. This investigation provides good guidance for the future rational design of high-performance PhOLED hosts by accumulative structural modifications.

Received 13th January 2015  
Accepted 9th March 2015

DOI: 10.1039/c5ra00694e

[www.rsc.org/advances](http://www.rsc.org/advances)

## 1. Introduction

Phosphorescent organic light-emitting diodes (PhOLEDs) have attracted intense interest because they can approach 100% internal quantum efficiency by utilizing both singlet and triplet excitons,<sup>1,2</sup> and are competing with fluorescent tube and inorganic LEDs as the next-generation illumination technology. To achieve high efficiency of PhOLEDs, phosphorescent emitters of heavy-metal complexes are usually doped into a suitable host matrix to suppress detrimental effects, such as aggregation quenching and triplet–triplet annihilation.<sup>3</sup> In recent years, universal RGB hosts that can host different-colored blue, green and red phosphors have attracted much attention due to their great potential for the simple and cost-effective fabrication of highly efficient, all-phosphor, single-emitting-layer, white

organic light-emitting diodes (WOLEDs) for full-color, flat panel displays and solid-state lighting.<sup>4</sup> Universal hosts with blue PhOLED EQEs of over 20% have been reported by several groups.<sup>5–7</sup>

However, to date, reports on universal RGB hosts, especially those with low driving voltages and high device efficiencies, are still limited.<sup>5–15</sup> This is because the molecular design of desirable universal host materials is difficult. In one aspect, a  $T_1$  higher than blue phosphor ( $>2.7$  eV) generally signifies a large energy bandgap, *i.e.*, a low-lying highest occupied molecular orbital (HOMO) level and/or a high-lying lowest occupied molecular orbital (LUMO) level, which may cause large energy barriers between adjacent layers in PhOLEDs and thus make charge carrier injection difficult and necessitate high driving voltages, thus greatly constraining their use for portable applications, such as mobile communications and consumer electronics. In another aspect, excessive tuning of FMO energy levels of universal hosts could result in the loss of the hosting abilities of one or more low-energy colored phosphors, due to the possible energy level mismatch, and thus impede energy transfer between the host and the phosphors.

Therefore, to obtain an efficient universal host for RGB phosphors, a compromise must be reached between high  $T_1$  and fine tuning of frontier molecular orbitals (FMOs). However, the tuning of HOMO/LUMO energy levels (determining the electrical properties, such as carrier injection ability) caused by molecular modifications usually simultaneously alters the HOMO/LUMO bandgaps ( $E_g$ ), and thus changes both the  $S_1$  and

<sup>a</sup>Key Laboratory for Organic Electronics and Information Displays & Institute of Advanced Materials (IAM), Jiangsu National Synergistic Innovation Center for Advanced Materials (SICAM), Nanjing University of Posts & Telecommunications, Nanjing, 210046, China. E-mail: iamhxie@njupt.edu.cn; iamwhuang@njupt.edu.cn

<sup>b</sup>State Key Laboratory on Integrated Optoelectronics, College of Electronic Science and Engineering, Jilin University, 2699 Qianjin Street, Changchun 130012, China. E-mail: zhao\_yi@jlu.edu.cn

<sup>c</sup>Key Laboratory of Flexible Electronics (KLOFE) & Institute of Advanced Materials (IAM), Jiangsu National Synergistic Innovation Center for Advanced Materials (SICAM), Nanjing Tech University, 30 South Puzhu Road, Nanjing 211816, China

† Electronic supplementary information (ESI) available: The CIE coordinates versus the luminance of the RGB devices. See DOI: 10.1039/c5ra00694e

‡ These authors, Y. Qian, Y. R. Ni and S. Z. Yue, contributed equally.

$T_1$  (determining the optical properties of whether the energy transfer from the host to phosphor can effectively occur). This intrinsic contradiction between optical and electrical properties often induces an uncontrollable adjustment of multiple properties. It remains a big challenge to simultaneously realize a high  $T_1$  for exothermic energy transfer and finely tunable FMO energy levels for balanced carrier injection and low operating voltages.

Ingenious construction of state-of-the-art models of electrophosphorescent hosts to uncover the deep role of each molecular modification in PhOLEDs performance is crucial for purposely cumulative improvement of device efficiency and for accelerating their commercialization. To overcome the intrinsic contradiction between optical and electrical properties, the selective modulation of a single optoelectronic characteristic, without changing other properties, has become an urgent issue for the rational design of high-performance organic hosts. It is believed that the modulation of a single property is more important than that of multiple properties, because in this way the uncontrollable and unexpected change of device performance caused by simultaneous variations of multiple properties can effectively be avoided. Xu reported a short-axis substitution approach of dibenzothiophene-based phosphine oxide (PO) blue and yellow hosts, which allows for selectively tuning the LUMO level by  $\sim 0.09$  eV without affecting the HOMO level and the  $T_1$ .<sup>16</sup> Thus, selective modification of the electron injection (EI) and electron transportation (ET) without affecting the hole injection (HI), hole transportation (HT) and  $T_1$  level has been realized. They also developed a series of ternary PO-dibenzofuran-carbazoly blue hosts by mixed meso and short-axis linkages<sup>17</sup> and another series of ternary PO-fluorene-carbazoly blue hosts through indirect linkage,<sup>17</sup> to controllably reduce  $S_1$  but keep  $T_1$  constant by simultaneously enhancing the HOMO levels and decreasing the LUMO levels (both within 0.1 eV), which facilitates both HT/HI and ET/EI. All these works provide effective methods for selective single tuning of electrical properties without changing  $T_1$  to achieve better device performance.

On this basis, it will be of more importance to realize multiple selective tuning of various single electrical properties without sacrificing the optical properties (such as  $T_1$ ) in the same series of hosts, because it helps to determine which factors among many are beneficial (positive effects) for improving device performance and which ones are not (negative effects). Thus, device efficiency can further be accumulatively improved through purposive and feasible modifications, one by one. In addition, it can also help to determine which positive factors are more effective and which negative factors are more detrimental to improving device performance, and thus provides better guidance for the molecular design in that which structural modifications are the top priorities. However, this multiple selective tuning of various single electrical properties through various structural modifications without affecting the optical properties is even more difficult than the above mentioned single selective tuning of electrical properties, and has seldom been reported.

In this present work, a series of spiro[fluorene-9,9'-xanthene](SFX)/9-arylfluorenes (AFs) hybrid universal RGB hosts have

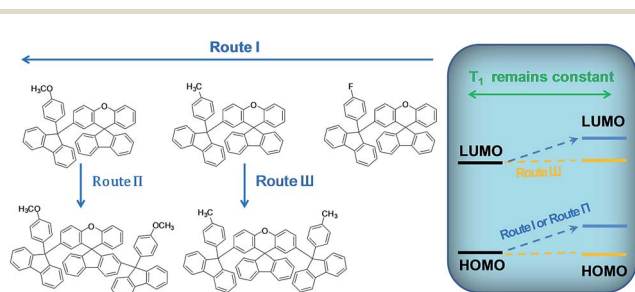
been developed *via* unconjugated linkage of SFX and various AFs, by utilizing our previously reported mild room temperature Friedel–Crafts reaction.<sup>18</sup> By varying the number, electronegativity and position of the bulky AF substitutes, the  $T_1$  for all the materials remains almost unchanged, but the latter two modifications have been demonstrated to realize respective tuning of the HOMO/LUMO energy levels (Scheme 1). This multiple selective tuning of electrical properties without sacrificing the high  $T_1$  can explain the performance of the corresponding RGB PhOLEDs. This work provides highly valuable design principles for developing more efficient universal RGB hosts through accumulative structural modifications.

## 2. Experimental section

### 2.1 Materials

SFX was synthesized by our previously reported method,<sup>25</sup> and the tertiary AFOHs were synthesized by an addition reaction of various phenyl Grignard reagents to fluorenone. SFX/AFs hybrid hosts were synthesized by the  $\text{MeSO}_3\text{H}$ -mediated Friedel–Crafts reaction of the tertiary AFOHs with the SFX.<sup>18</sup>

**2'-(9-(4-Methoxyphenyl)-fluoren-9-yl)spiro[fluorene-9,9'-xanthene] (MOAF-SFX).**  $\text{MeSO}_3\text{H}$  (1.20 ml, 9.04 mmol) was added to 15 ml of an anhydrous  $\text{CH}_2\text{Cl}_2$  solution of SFX (1.0 g, 3.01 mmol) and 9-(4-methoxyphenyl)-fluoren-9-ol (1.74 g, 6.02 mmol), and the batch was stirred over a period of 5 h at room temperature. The resulting mixture was washed with water and extracted with  $\text{CH}_2\text{Cl}_2$ . The combined organic layers were then subjected to silica-gel column chromatography to afford 0.45 g of white solid in a 24.8% yield.  $^1\text{H}$  NMR (400 MHz,  $\text{CDCl}_3$ ,  $\delta$ ): 7.69–7.67 (d,  $J = 7.2$  Hz, 2H, Ar H), 7.64–7.62 (d,  $J = 7.6$  Hz, 2H, Ar H), 7.34–7.30 (td,  $J = 7.2$  Hz, 1.2 Hz, 2H, Ar H), 7.24–7.21 (m, 2H, Ar H), 7.20–7.12 (m, 4H, Ar H), 7.14–7.12 (d,  $J = 7.2$  Hz, 2H, Ar H), 7.09–7.05 (td,  $J = 7.6$  Hz, 1.2 Hz, 2H, Ar H), 7.00–6.96 (d,  $J = 8.8$  Hz, 1H, Ar H), 6.91–6.89 (d,  $J = 8$  Hz, 2H, Ar H), 6.84–6.81 (dd,  $J = 8.4$  Hz, 2.4 Hz, 1H, Ar H), 6.78–6.74 (m,  $J = 1.2$  Hz, 1H, Ar H), 6.70–6.67 (dt,  $J = 9.2$  Hz, 2.8 Hz, 2H, Ar H), 6.49–6.47 (dt,  $J = 8.8$  Hz, 2.6 Hz, 2H, Ar H), 6.44–6.42 (d,  $J = 8.4$  Hz, 1H, Ar H), 6.38–6.37 (d,  $J = 2.4$  Hz, 1H, Ar H), 3.68 (s, 3H,  $\text{CH}_3$ );  $^{13}\text{C}$  NMR (400 MHz,  $\text{CDCl}_3$ ,  $\delta$ ): 157.92, 155.18, 151.59, 151.47, 150.03, 140.10, 139.84, 139.60, 137.74, 128.88, 128.74, 128.15, 128.10, 127.63, 127.53, 127.34, 127.18, 125.74, 125.57, 124.63, 124.61, 123.24, 119.97, 119.90, 116.77, 116.19, 113.23, 63.90, 55.16, 54.32; MALDI-TOF



Scheme 1 Multiple selective tuning of electrical properties whilst keeping the  $T_1$  constant *via* various structural modifications.

(*m/z*): 602.75 [M]<sup>+</sup>; Anal. calcd for C<sub>45</sub>H<sub>30</sub>O<sub>2</sub> (602.72): C 89.67, H 5.02; found: C 89.88, H 4.96.

**2,2'-Bis(9-(4-methoxyphenyl)-fluoren-9-yl)spiro[fluorene-9,9'-xanthene] (DMOAF-SFX).** The synthesis was similar to that of MOAF-SFX. The residue was purified through silica-gel column chromatography to yield 0.34 g of white solid in a 12.9% yield. <sup>1</sup>H NMR (400 MHz, CDCl<sub>3</sub>, δ): 7.72–7.70 (d, *J* = 7.6 Hz, 2H, Ar H), 7.59–7.58 (d, *J* = 7.2 Hz, 2H, Ar H), 7.51–7.49 (d, *J* = 7.2 Hz, 2H, Ar H), 7.36–7.32 (td, *J* = 7.6 Hz, 0.8 Hz, 2H, Ar H), 7.23–7.20 (t, *J* = 6.8 Hz, 5H, Ar H), 7.18–7.13 (m, 6H, Ar H), 7.09–7.07 (d, *J* = 7.6 Hz, 3H, Ar H), 6.98–6.94 (m, 3H, Ar H), 6.84–6.78 (m, 3H, Ar H), 6.79–6.78 (d, *J* = 7.2 Hz, 3H, Ar H), 6.71–6.67 (m, 3H, Ar H), 6.46–6.42 (m, 3H, Ar H), 6.14–6.14 (d, *J* = 2 Hz, 1H, Ar H), 3.65 (s, 3H, CH<sub>3</sub>), 3.24 (s, 3H, CH<sub>3</sub>); <sup>13</sup>C NMR (400 MHz, CDCl<sub>3</sub>, δ): 157.55, 156.81, 154.95, 151.77, 151.51, 150.27, 149.95, 140.99, 139.86, 139.75, 139.59, 137.85, 137.60, 133.15, 132.58, 129.73, 128.35, 128.13, 128.11, 127.98, 127.59, 127.35, 127.29, 127.23, 127.22, 126.91, 126.12, 125.81, 125.66, 124.89, 124.40, 123.20, 121.05, 119.75, 119.67, 119.56, 63.67, 63.17, 55.31, 55.12, 54.37; MALDI-TOF (*m/z*): 982.27 [M + Ag]<sup>+</sup>; Anal. calcd for C<sub>65</sub>H<sub>44</sub>O<sub>3</sub> (873.04): C 89.42, H 5.08; found: C 89.58, H 5.12.

**2'-(9-*p*-Tolyl-fluoren-9-yl)spiro[fluorene-9,9'-xanthene] (MAF-SFX).** The synthesis was similar to that of MOAF-SFX. The residue was purified through silica-gel column chromatography to yield 0.73 g of white solid in a 41.5% yield. <sup>1</sup>H NMR (400 MHz, CDCl<sub>3</sub>, δ): 7.68–7.66 (d, *J* = 7.6 Hz, 2H, Ar H), 7.64–7.62 (d, *J* = 7.2 Hz, 2H, Ar H), 7.34–7.30 (td, *J* = 7.2 Hz, 1.2 Hz, 2H, Ar H), 7.26–7.22 (t, *J* = 7.6 Hz, 2H, Ar H), 7.21–7.17 (m, 4H, Ar H), 7.15–7.14 (d, *J* = 7.2 Hz, 2H, Ar H), 7.09–7.05 (td, *J* = 7.6 Hz, 1.2 Hz, 2H, Ar H), 7.02–7.00 (d, *J* = 8.4 Hz, 1H, Ar H), 6.94–6.92 (d, *J* = 7.6 Hz, 2H, Ar H), 6.89–6.87 (dd, *J* = 8.8 Hz, 2.4 Hz, 1H, Ar H), 6.79–6.75 (m, 3H, Ar H), 6.69–6.67 (d, *J* = 8 Hz, 2H, Ar H), 6.45–6.44 (d, *J* = 7.6 Hz, 1H, Ar H), 6.372–6.366 (d, *J* = 2.4 Hz, 1H, Ar H), 2.20 (s, 3H, CH<sub>3</sub>); <sup>13</sup>C NMR (400 MHz, CDCl<sub>3</sub>, δ): 155.06, 151.58, 151.29, 150.02, 142.67, 139.98, 139.88, 139.56, 135.66, 128.81, 128.54, 128.10, 128.06, 128.04, 127.56, 127.52, 127.47, 127.43, 127.12, 125.76, 125.53, 124.69, 124.57, 123.19, 119.91, 119.82, 116.73, 116.14, 64.20, 54.31, 20.82; MALDI-TOF (*m/z*): 586.93 [M]<sup>+</sup>; Anal. calcd for C<sub>45</sub>H<sub>30</sub>O (586.72): C 92.12, H 5.15; found: C 92.22, H 5.08.

**2',7'-Bis(9-*p*-tolyl-fluoren-9-yl)spiro[fluorene-9,9'-xanthene] (DMAF-SFX).** The synthesis was similar to that of MOAF-SFX. The residue was purified through silica-gel column chromatography to yield 0.50 g of white solid in a 19.6% yield. <sup>1</sup>H NMR (400 MHz, CDCl<sub>3</sub>, δ): 7.63–7.61 (d, *J* = 7.6 Hz, 4H, Ar H), 7.55–7.53 (d, *J* = 7.6 Hz, 2H, Ar H), 7.28–7.21 (m, 6H, Ar H), 7.18–7.15 (t, *J* = 6.8 Hz, 2H, Ar H), 7.11–7.10 (d, *J* = 7.2 Hz, 2H, Ar H), 7.07–7.04 (d, *J* = 7.6 Hz, 4H, Ar H), 6.97–6.95 (d, *J* = 8.4 Hz, 2H, Ar H), 6.93–6.91 (d, *J* = 7.6 Hz, 4H, Ar H), 6.85–6.82 (dd, *J* = 8.8 Hz, 2.4 Hz, 2H, Ar H), 6.76–6.74 (d, *J* = 8 Hz, 4H, Ar H), 6.67–6.65 (d, *J* = 8 Hz, 4H, Ar H), 6.40–6.39 (d, *J* = 2.4 Hz, 2H, Ar H), 2.18 (s, 6H, CH<sub>3</sub>); <sup>13</sup>C NMR (400 MHz, CDCl<sub>3</sub>, δ): 154.96, 151.35, 150.28, 142.71, 139.89, 139.50, 135.66, 128.91, 128.53, 127.82, 127.52, 127.47, 127.39, 127.32, 127.11, 125.79, 125.33, 124.51, 119.90, 119.74, 116.14, 64.23, 54.47, 20.82; MALDI-TOF (*m/z*): 841.24 [M + H]<sup>+</sup>; Anal. calcd for C<sub>65</sub>H<sub>44</sub>O (840.34): C 92.82, H 5.27; found: C 92.71, H 5.34.

**2'-(9-(4-Fluorophenyl)-fluoren-9-yl)spiro[fluorene-9,9'-xanthene] (FAF-SFX).** The synthesis was similar to that of MOAF-SFX. The residue was purified through silica-gel column chromatography to yield 0.75 g of white solid in a 42.2% yield. <sup>1</sup>H NMR (400 MHz, CDCl<sub>3</sub>, δ): 7.70–7.68 (d, *J* = 7.6 Hz, 2H, Ar H), 7.65–7.63 (d, *J* = 7.6 Hz, 2H, Ar H), 7.36–7.33 (t, *J* = 7.2 Hz, 2H, Ar H), 7.28–7.18 (m, 6H, Ar H), 7.14–7.12 (d, *J* = 7.6 Hz, 2H, Ar H), 7.10–7.07 (t, *J* = 6.8 Hz, 2H, Ar H), 6.99–6.97 (d, *J* = 8.4 Hz, 1H, Ar H), 6.88–6.86 (d, *J* = 8 Hz, 2H, Ar H), 6.79–6.71 (m, 4H, Ar H), 6.64–6.60 (t, *J* = 8.4 Hz, 2H, Ar H), 6.46–6.44 (d, *J* = 7.6 Hz, 1H, Ar H), 6.352–6.346 (d, *J* = 2.4 Hz, 1H, Ar H); <sup>13</sup>C NMR (400 MHz, CDCl<sub>3</sub>, δ): 155.19, 151.52, 150.99, 150.07, 139.84, 139.70, 139.56, 129.19, 129.19, 128.93, 128.20, 128.15, 128.13, 127.70, 127.62, 127.39, 127.06, 125.68, 125.53, 124.82, 124.42, 123.28, 120.07, 119.89, 116.76, 116.23, 114.65, 114.44, 63.92, 54.26; MALDI-TOF (*m/z*): 590.692 [M]<sup>+</sup>; Anal. calcd for C<sub>44</sub>H<sub>27</sub>FO (590.68): C 89.47, H 4.61; found: C 89.67, H 4.72.

## 2.2 Instrumental methods

The NMR spectra were recorded on a Bruker AV 400 MHz NMR spectrometer. Mass spectra were collected using a Microflex MALDI-TOF mass-spectrometer (Bruker Daltonics, Germany). UV-vis absorption and photoluminescence spectra were recorded with a Shimadzu UV-3600 and a Shimadzu RF-5301PC spectrophotometer, respectively. Differential scanning calorimetry (DSC) and thermogravimetric analyses (TGA) were performed on a Shimadzu DSC-60A and a Shimadzu DTG-60H, respectively. Cyclic voltammetric (CV) studies were conducted using an Eco Chemie B. V. Autolab potentiostat.

## 2.3 Theoretical computation methods

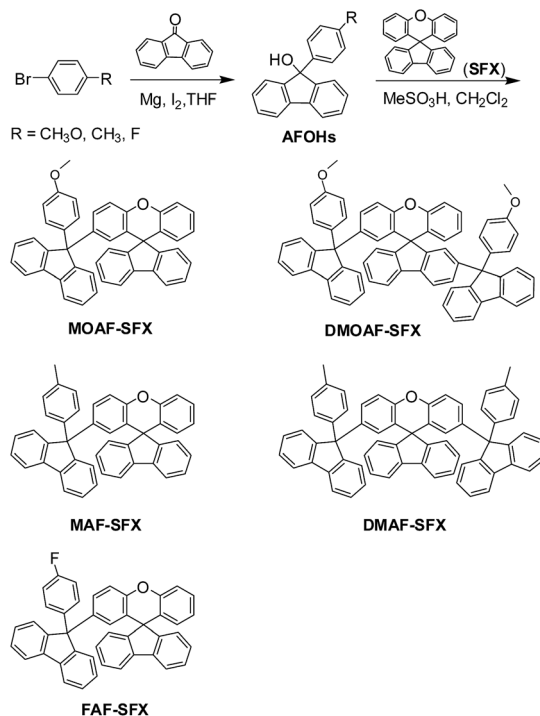
Geometrical optimization for the ground and excited states was carried out at the B3LYP/6-31G and CIS/6-31G levels, respectively. The TDDFT/B3LYP/6-31g calculations of the excitation energies were then performed at the optimized geometries. All the quantum-chemical calculations were performed using the Gaussian 09 suite of programs.<sup>26</sup>

# 3. Results and discussion

## 3.1 Synthesis and characterization

SFX/AFs hybrid compounds have been synthesized *via* two simple steps by the very mild room temperature MeSO<sub>3</sub>H-mediated Friedel–Crafts reaction<sup>18</sup> of the tertiary alcohols of 9-aryl-fluoren-9-ols (AFOHs) with the SFX followed by the addition reaction of various phenyl Grignard reagents to fluorenone (Scheme 2), from which three kinds of products – single AF-substituted, symmetrically double AF-substituted, and asymmetrically double AF-substituted SFX derivatives – can be obtained.

The former addition reaction of the various phenyl Grignard reagents with fluorenone allows for easy tuning of the electro-negativity of the substitutions (CH<sub>3</sub>O, CH<sub>3</sub>, F) on the phenyl rings in the AF moieties. The latter Friedel–Crafts reaction allows for one-step unconjugated connection between SFX and various AFs by the saturated sp<sup>3</sup>-C atom through single or



Scheme 2 Synthesis and molecular structures of SFX/AFs hybrid compounds.

double substitution, which is beneficial for maintaining both a large energy band ( $E_g$ ) and a high  $T_1$ . Thus, by varying the electronegativity of the AF substitutes, the substitution numbers or positions, the fine tuning of the FMO energy levels (mainly concerning electrical properties) without significant change of the  $E_g$  and  $T_1$  (mainly concerning optical properties) can be expected. In this work, five purified compounds have been obtained: 2'-(9-(4-methoxyphenyl)-fluoren-9-yl)spiro[fluorene-9,9'-xanthene] (MOAF-SFX), 2,2'-bis(9-(4-methoxyphenyl)-fluoren-9-yl)spiro[fluorene-9,9'-xanthene] (DMOAF-SFX), 2'-(9-*p*-tolyl-fluoren-9-yl)spiro[fluorene-9,9'-xanthene] (MAF-SFX), 2',7'-bis(9-*p*-tolyl-fluoren-9-yl)spiro[fluorene-9,9'-xanthene] (DMAF-SFX), and 2'-(9-(4-fluorophenyl)-fluoren-9-yl)spiro[fluorene-9,9'-xanthene] (FAF-SFX). All these compounds have been fully characterized by <sup>1</sup>H NMR, <sup>13</sup>C NMR, MALDI-TOF MS spectroscopy and elemental analysis (Fig. S1–5<sup>†</sup>).

### 3.2 Thermal properties

The thermal properties of the SFX/AFs compounds were investigated by thermogravimetric analysis (TGA) and differential scanning calorimetry (DSC) (Fig. 1). All the five compounds exhibit high thermal decomposition temperatures ( $T_d$ ) in the range of 356–436 °C. As indicated in the DSC curves, no significant signals of glass transition temperature ( $T_g$ ) were observed, except that the  $T_g$  of FAF-SFX was detected at about 171 °C. The melting points ( $T_m$ ) of DMAF-SFX and FAF-SFX can be derived from the DSC curves to be 360 and 268 °C, respectively. In general, the double AF-substituted compounds of DMOAF (423 °C) and DMAF-SFX (436 °C) exhibit higher  $T_d$  values than the mono AF-substituted compounds of MOAF-SFX

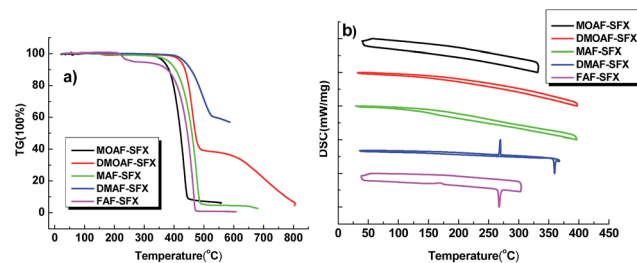


Fig. 1 TGA (a) and DSC (b) curves of SFX/AFs hybrid compounds recorded at a heating/cooling rate of 5 °C min<sup>-1</sup>.

(366 °C), MAF-SFX (383 °C) and FAF-SFX (410 °C). For the mono AF-substituted compounds, with increasing electronegativity of the substituents on the phenyl ring in the AF moieties (from CH<sub>3</sub>O for MOAF-SFX, CH<sub>3</sub> for MAF-SFX, to F for FAF-SFX), the  $T_d$  increased. This good thermal performance was probably due to the steric hindrance caused by the spiro-configuration, which effectively reduces the intermolecular aggregation. Thus, it gives these compounds advantageous film morphology stability and suppresses the phase separation during device operation.

### 3.3 Photophysical properties

Fig. 2 shows the absorption and fluorescence spectra of the SFX/AFs hybrid compounds in dilute acetonitrile solutions and as thin films, respectively. In the solutions, the maximum absorption peaks at around 261–265 nm are mainly attributed to the  $\pi$ - $\pi^*$  transition of the SFX and AFs moieties. The small absorptions in the longer-wavelength region at 293–295 nm and 305–307 nm are possibly due to some extension of intramolecular charge transfer, consistent with the FMO charge distributions, which will be discussed below.

The two emission peaks in the solutions are in the range of 312–320 nm and 322–328 nm, which possibly originate from the  $\pi$ - $\pi^*$  transitions of AFs and SFX. In the thin films, probably due to the some degree of intermolecular aggregation, the long-wavelength absorptions at around 290–310 nm increase and become comparable with the absorptions at around 261–265 nm. Consistently, the emissions in films are red-shifted by 20–30 nm as compared with their solutions. Their phosphorescence spectra were measured in CH<sub>2</sub>Cl<sub>2</sub> matrix at 77 K (Fig. 3), in which  $T_1$  was estimated from the highest energy vibronic sub-bands. All of the compounds exhibit high  $T_1$  with almost identical values of 2.87–2.88 eV, which are sufficiently

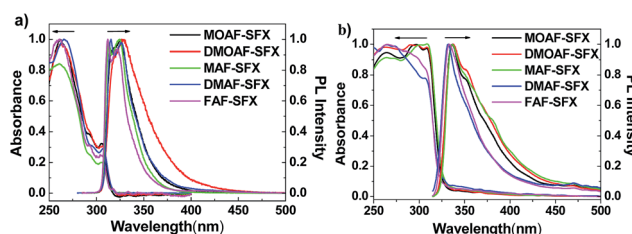


Fig. 2 UV-vis absorption and PL spectra of SFX/AFs hybrid compounds in solutions (a) and as thin films (b).

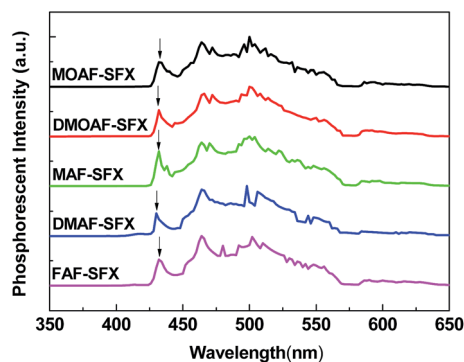


Fig. 3 The phosphorescence spectra of SFX/AFs hybrid compounds in  $\text{CH}_2\text{Cl}_2$  matrix at 77 K.

high to confine the triplet excitons of the blue phosphor of iridium(III) bis(4,6-(difluorophenyl)pyridine-*N,C2'*) picolinate (FIrpic,  $T_1 = 2.65$  eV).

### 3.4 Tunable frontier molecular orbitals and electrical properties

Cyclic voltammetry (CV) was performed to investigate the electrochemical properties of the SFX/AFs hybrid compounds (Fig. 4). During the anodic scan in  $\text{CH}_2\text{Cl}_2$ , all these compounds exhibit one quasi-reversible, one-electron oxidation process, from which the HOMO energy levels can be derived. The LUMO energy levels can be calculated from the values of HOMO energy levels and the optical energy band gaps, which are determined from the absorption onset. As anticipated, both the HOMO and LUMO energy levels fall in the relatively small ranges of  $-6.10$ – $5.94$  eV and  $-2.15$ – $2.02$  eV, respectively. The  $E_g$  values of the SFX/AFs hybrid compounds are in proximity ( $3.92$ – $3.95$  eV), which is in good agreement with their similar photophysical parameters and  $T_1$  values.

The physical data, including  $T_g$ ,  $T_d$ , absorption and emission wavelengths, HOMO/LUMO values,  $E_g$  and  $T_1$ , are all summarized in Table 1. From these data, several conclusions can be drawn: (1) whatever the modification to the electronegativity, the substitution numbers or the substitution position of the AF substituents,  $T_1$  exhibits almost no change for all these compounds at  $2.87$ – $2.88$  eV. (2) By decreasing the

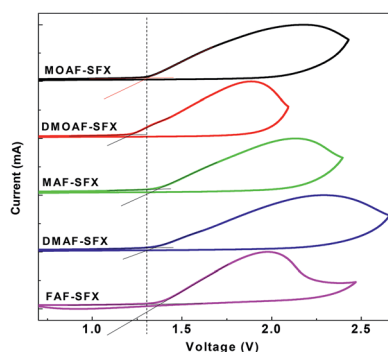


Fig. 4 Cyclic voltammograms of the oxidation for SFX/AFs hybrid compounds in  $\text{CH}_2\text{Cl}_2$ .

electronegativity of the phenyl substitutes in the AF moieties, the HOMO and LUMO energy levels simultaneously increased with both the  $E_g$  and  $T_1$  remaining almost constant. For the monosubstituted FAF-SFX, MAF-SFX and MOAF-SFX, with the sequence in electronegativity of fluorophenylfluorene > tolylfluorene > methoxyphenylfluorene, the HOMO and LUMO energy levels simultaneously increased. The HOMO energy levels of FAF-SFX, MAF-SFX and MOAF-SFX are  $-6.10$ ,  $-6.08$  and  $-6.03$  eV, respectively, while the LUMO energy levels are  $-2.15$ ,  $-2.14$  and  $-2.09$  eV, respectively. Although the tuning from tolylfluorene substituted MAF-SFX to methoxyphenylfluorene substituted MOAF-SFX is small, the relatively large tuning from fluorophenylfluorene substituted FAF-SFX to methoxyphenylfluorene substituted MOAF-SFX proves that this tuning of HOMO/LUMO levels by changing electronegativity does work. (3) From the mono methoxyphenylfluorene substituted MOAF-SFX to the double asymmetrically substituted DMOAF-SFX, the HOMO and LUMO energy levels are simultaneously elevated by  $0.09$  eV and  $0.07$  eV, respectively, with  $T_1$  remaining constant. The HOMO energy levels of MOAF-SFX and DMOAF-SFX are  $-6.03$  and  $-5.94$  eV, respectively, while the LUMO energy levels are  $-2.09$  and  $-2.02$  eV, respectively. (4) From the mono tolylfluorene substituted MAF-SFX to the double symmetrically substituted DMAF-SFX, both the HOMO and LUMO energy levels remain almost constant.

Therefore, either by decreasing the electronegativity of the AF substituents (Route I) or introducing asymmetrical substitution (Route II), the HOMO and/or LUMO energy levels are enhanced and thus the hole injecting and/or electron blocking will be facilitated without affecting the  $T_1$ . Thus, FAF-SFX exhibits the lowest HOMO/LUMO energy levels, while DMOAF-SFX, with accumulative modifications of Route I and Route II (see Scheme 1), exhibits the highest HOMO/LUMO energy levels. This multiple selective fine tuning of electrical properties, without sacrifice of optical properties, is very helpful for understanding how each modification can affect the subsequent device performance and which factors can cause the most prominent impact.

Nevertheless, whether changing the electronegativity of the AF substitutes or changing the substitution positions, these structural modifications are insulated by the spiro  $\text{sp}^3\text{-C}$  atoms in both the SFX moiety and on the 9-position of the AF moieties. How these structural modifications effectively affect, across the insulated segments, the FMO energy levels needs further investigation. Thus, the DFT calculations were performed for these compounds. It is interesting to find that, unlike most previously published hosts in which the charge distributions on the HOMO and the LUMO are mainly located on the donor/HT and acceptor/ET moieties, respectively, this series of SFX/AFs hybrid compounds exhibits an unusual shift of FMO charge distributions with the same parent segments of SFX and AFs (Fig. 5).

Several comparisons are conducted as follows: (1) for the mono AF-substituted MOAF-SFX, MAF-SFX, and FAF-SFX, although the charge distributions on the HOMO orbitals are similarly located on the xanthene ring and the fluorene ring in the AFs, the charge distributions on the LUMO orbitals are quite

Table 1 The physical parameters of SFX/AFs hybrid compounds

Compound	$T_g^a$ (°C)	$T_d^b$ (°C)	$\lambda_{\text{abs}}$ (nm)	$\lambda_{\text{em}}$ (nm)	HOMO/LUMO <sup>c</sup> (eV)	$E_g^d$ (eV)	$T_1^e$ (eV)	$\tau^f$ (ns)	$Q_t^g$
MOAF-SFX	—	366	262, 293 <sup>s</sup> , 305 <sup>h</sup> 265, 297, 308 <sup>i</sup>	317 <sup>s</sup> , 325 <sup>h</sup> 337, 352 <sup>si</sup>	−6.026/−2.090	3.936	2.87	1.1	0.5%
DMOAF-SFX	—	423	264, 293 <sup>s</sup> , 306 <sup>h</sup> 263, 293, 309 <sup>i</sup>	320 <sup>s</sup> , 328 <sup>h</sup> 338, 352 <sup>i</sup>	−5.937/−2.017	3.920	2.87	1.1	0.6%
MAF-SFX	—	383	261, 294 <sup>s</sup> , 306 <sup>h</sup> 265, 302, 309 <sup>i</sup>	313, 324 <sup>h</sup> 337, 350 <sup>i</sup>	−6.084/−2.144	3.940	2.87	2.1	0.8%
DMAF-SFX	—	436	266, 295 <sup>s</sup> , 307 <sup>h</sup> 265, 288, 306 <sup>i</sup>	315, 326 <sup>h</sup> 332, 348 <sup>si</sup>	−6.071/−2.145	3.925	2.88	3.6	1.2%
FAF-SFX	171	410	261, 293 <sup>s</sup> , 306 <sup>h</sup> 264, 289, 307 <sup>i</sup>	312, 322 <sup>h</sup> 333, 352 <sup>si</sup>	−6.100/−2.149	3.950	2.87	3.5	0.8%

<sup>a</sup> Obtained from DSC measurements. <sup>b</sup> Obtained from TGA measurements. <sup>c</sup> HOMO levels were measured from the onset of oxidation potentials in CH<sub>2</sub>Cl<sub>2</sub>, LUMO levels was deduced from HOMO and  $E_g$ . <sup>d</sup> Estimated from the absorption edges. <sup>e</sup> Determined from the phosphorescence spectra in CH<sub>2</sub>Cl<sub>2</sub> at 77 K. <sup>f</sup> Lifetime (see Fig. S6). <sup>g</sup> Quantum yields in powder. <sup>h</sup> Measured in acetonitrile solutions. <sup>i</sup> Measured in thin films; “s” means shoulder peaks; “—” means no observation of obvious  $T_g$  signals.

different. For MOAF-SFX, the LUMO orbital is mainly distributed on the two fluorenes from the SFX and AF moiety. For MAF-SFX, the charge on the LUMO is mainly distributed on the fluorene from the SFX moiety, while for FAF-SFX it is mainly distributed on the fluorene from the AF moiety. (2) For the double substituted DMOAF-SFX and DMAF-SFX, the charge distributions of both the HOMO and the LUMO are quite different. For the asymmetrically double methoxyphenyl-fluorene substituted DMOAF-SFX, the HOMO orbital is mainly located on the SFX and the two fluorenes in the two AFs substitutes, while the LUMO orbital is mainly distributed on the fluorene in the SFX and the fluorene in the xanthene-linked AF. For the symmetrically double tolylfluorene substituted DMAF-SFX, the HOMO orbital is mainly located on the SFX unit (with little charge distribution on the fluorenes of the two AF substitutes), while the LUMO orbital is mainly distributed on the two fluorenes of the two AF substitutes. (3) For the mono- and double asymmetrically methoxyfluorene substituted MOAF-SFX and DMOAF-SFX, the charge distribution on the FMOs is different as well. For the HOMO, the charge is mainly located on the xanthene ring in the SFX and the fluorene in the AF for MOAF-SFX, while it is located on the whole SFX unit and the fluorene in the spiro-fluorene-linked AF substitute for DMOAF-SFX (the charge on the fluorene in the xanthenes-linked AF is very small). For the LUMO, the charge for MOAF-SFX is mainly located on the two fluorenes from the SFX and the AF, and for DMOAF-SFX on the fluorene from the SFX

and the fluorene from the xanthenes-linked AF. (4) For the mono- and double symmetrically tolylfluorene substituted MAF-SFX and DMAF-SFX, the charge distribution on the FMOs also varies. For the HOMO, the charge is mainly located on the xanthene ring in the SFX and the fluorene ring in the AF for MAF-SFX, while mainly on the xanthene in the SFX (with very little charge distributed on the two fluorenes on the AF substitutes) for DMAF-SFX. For the LUMO, the charge distributes on the fluorene in the SFX for MAF-SFX and on the two fluorenes from the AF substitutes for DMAF-SFX. It is regarded that the above mentioned two methods for selective fine tuning of the HOMO and LUMO energy levels with various structural modifications are possibly related to this unusual shifting of FMOs charge distributions.

### 3.5 Electroluminescent device performances

In view of the high triplet energies ( $T_1 = 2.87$ – $2.88$  eV) and the photophysical characteristics, the FIrpic-based blue phosphorescent devices B1–B5, hosted by MOAF-SFX, DMOAF-SFX, MAF-SFX, DMAF-SFX and FAF-SFX, respectively, are firstly fabricated to investigate how this multiple fine tuning of FMO levels can affect device performance. The device structures are ITO/MoO<sub>x</sub> (2 nm)/*m*-MTDATA : MoO<sub>x</sub> (3 : 1) (15 nm)/*m*-MTDATA (25 nm)/Ir(ppz)<sub>3</sub> (10 nm)/host:FIrpic (10 wt%, 10 nm)/3TPYMB (10 nm)/BPhen (30 nm)/LiF (1 nm)/Al (100 nm), where MoO<sub>x</sub> and LiF served as hole- and electron-injecting layers, *m*-MTDATA and BPhen as the HTL and ETL, Ir(ppz)<sub>3</sub> as hole transporting and electron-blocking material, 3TPYMB as the electron transporting layer and hole-blocking material, and FIrpic doped in the SFX/AFs hybrid hosts as the EML. Fig. 6 shows the current density–voltage–brightness ( $J$ – $V$ – $L$ ) characteristics and efficiency curves *versus* luminance. The driving voltages are remarkably lower than 3.0 V for onset and still lower than 4.0 V at a luminance of 100 cd m<sup>−2</sup>. Device B2 is hosted by DMOAF-SFX, which possesses the highest-lying HOMO (−5.94 eV) and LUMO (−2.02 eV) levels, and thus achieves the best electroluminescence performance with a maximum current efficiency (CE) of 25.3 cd A<sup>−1</sup>, PE of 21.6 lm W<sup>−1</sup> and EQE of 11.9%. This is because the doping of FIrpic can

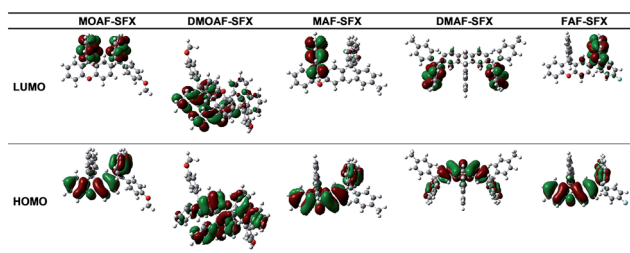


Fig. 5 The calculated charge spatial distributions on the HOMOs and the LUMOs of the SFX/AFs hybrid compounds.

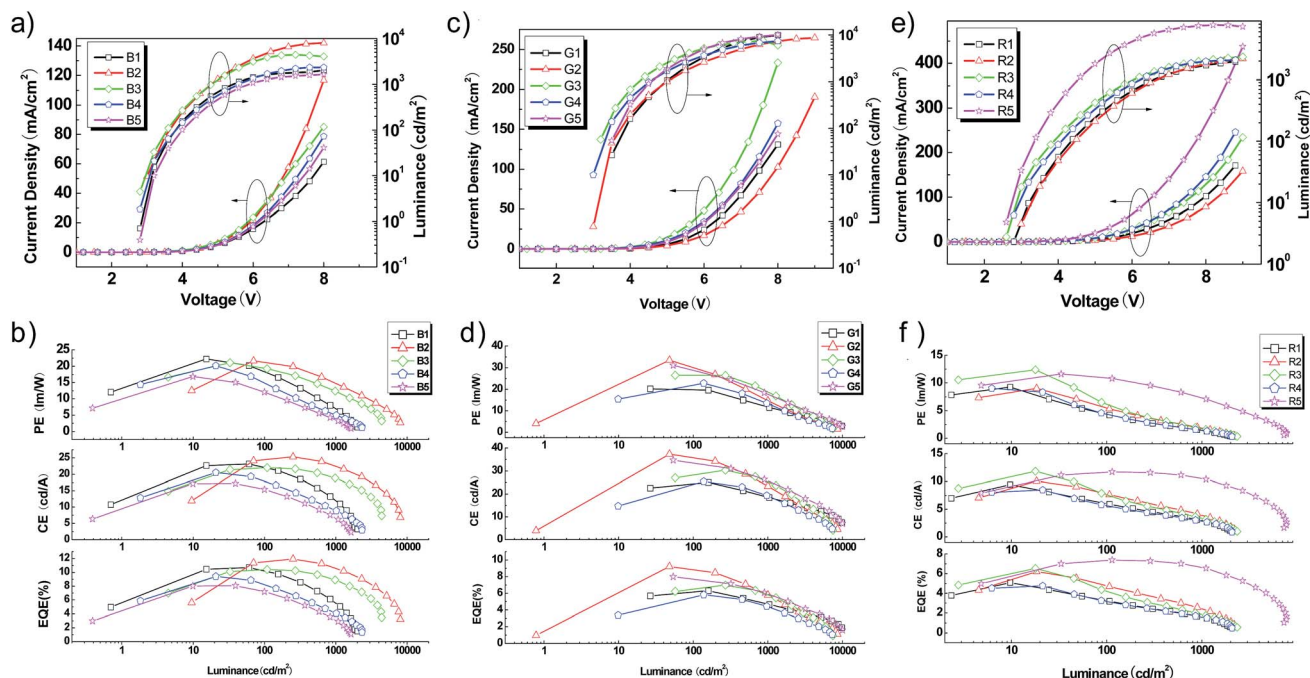


Fig. 6  $J$ - $V$ - $L$  characteristics (a, c, e) and efficiency curves (b, d, f) of the blue, green and red PhOLEDs hosted by the SFX/AFs hybrid compounds.

dramatically enhance the electron transporting characteristic in EML,<sup>19,20</sup> and thus a higher HOMO/LUMO energy level facilitated hole injection/electron blocking and better balanced charge injection/transportation. Consistently, device B2 exhibits a lower efficiency roll-off of 9.4% at a brightness of  $1000 \text{ cd m}^{-2}$  with EQE still as high as 10.6%. Besides, the color stabilities of all the devices are excellent, with almost no change in the Commission International de l'Eclairage (CIE) coordinates in the full range of the operating voltages (Fig. S7†).

The higher device efficiency of the blue PhOLEDs prompted us to further test the applicability of these hosts to green and red

phosphorescent emitters. The green (G1–G5) and red devices (R1–R5) are fabricated with almost the same device structure as the blue devices except for removing the hole blocking layer of 3TPymb, by using MOAF-SFX, DMOAF-SFX, MAF-SFX, DMAF-SFX and FAF-SFX as the hosts, respectively, and 8 wt% iridium(III) bis(2-phenylpyridinato- $N,C2'$ ) acetylacetonate [(ppy)<sub>2</sub>-Ir(acac)] and 6 wt% bis(2-methylidibenzo-[f, h]-quinoxaline) acetylacetonate iridium(III) [Ir(MDQ)<sub>2</sub>(acac)] as the green and red dopants, respectively. All the green and red PhOLEDs exhibit good color stabilities (Fig. S8 and 9†). The  $J$ - $V$ - $L$  characteristics and efficiency curves *versus* luminance (Fig. 6c–f) indicate that

Table 2 Electroluminescence performances of the SFX/AF-based PhOLEDs

Devices	$V_{\text{on}}^a$ [V]	$\text{CE}^b$ [ $\text{cd A}^{-1}$ ]	$\text{PE}^b$ [ $\text{lm W}^{-1}$ ]	$\text{EQE}_t^b$ [%]	CIE ( $x, y$ ) <sup>c</sup>
B1	2.8, 3.8	23.1, 22.1, 11.9	22.2, 18.2, 6.9	10.7, 10.2, 5.6	(0.15, 0.31)
B2	3.0, 3.6	25.3, 24.5, 22.4	21.6, 21.2, 14.7	11.9, 11.5, 10.6	(0.15, 0.34)
B3	2.8, 3.6	22.0, 22.0, 18.9	21.0, 19.4, 12.3	10.4, 10.4, 8.9	(0.15, 0.32)
B4	2.8, 3.8	20.5, 17.9, 9.0	20.1, 14.8, 5.0	9.4, 8.2, 4.1	(0.15, 0.32)
B5	2.8, 4.0	17.2, 15.4, 6.6	16.8, 12.0, 3.6	8.1, 7.2, 3.1	(0.15, 0.31)
G1	3.5, 3.9	25.0, 24.4, 18.6	20.2, 19.7, 11.8	6.3, 6.1, 4.7	(0.30, 0.64)
G2	3.0, 3.8	48.0, 35.7, 23.4	33.5, 30.1, 14.7	9.2, 8.8, 5.8	(0.30, 0.64)
G3	3.2, 3.3	30.3, 28.2, 25.2	26.5, 26.5, 18.8	7.0, 6.5, 5.8	(0.31, 0.64)
G4	3.0, 3.4	25.4, 24.1, 19.1	22.8, 21.9, 13.4	5.8, 5.5, 4.4	(0.31, 0.64)
G5	3.5, 3.7	34.7, 33.4, 25.8	31.1, 28.8, 17.8	8.0, 7.7, 5.9	(0.31, 0.64)
R1	2.8, 4.3	9.4, 6.0, 2.9	9.3, 4.3, 1.4	5.1, 3.2, 1.6	(0.60, 0.40)
R2	3.0, 4.4	10.1, 7.7, 3.9	9.0, 5.4, 1.8	6.2, 4.8, 2.4	(0.61, 0.39)
R3	2.8, 3.8	11.8, 5.6, 3.3	12.4, 6.2, 1.7	6.5, 4.2, 1.9	(0.60, 0.39)
R4	2.6, 4.0	8.5, 7.6, 2.8	9.0, 4.4, 1.4	4.8, 3.3, –	(0.61, 0.39)
R5	2.6, 3.3	11.7, 11.6, 10.5	11.6, 10.9, 7.9	7.4, 7.3, 6.2	(0.62, 0.38)
W	2.8, 4.2	18.9, 15.0, 6.3	16.9, 11.3, 3.2	7.6, 6.1, 2.6	(0.27, 0.38)

<sup>a</sup> Turn-on voltages and driving voltages at  $100 \text{ cd m}^{-2}$ . <sup>b</sup> Maximum values, then values at 100 and  $1000 \text{ cd m}^{-2}$ . <sup>c</sup> At 7 V.

the turn-on voltages of the green and red devices are lower than 3.5 and 3.0 V, respectively, and at a luminance of  $100 \text{ cd m}^{-2}$  the driving voltages are still lower than 4.0 and 4.5 V, respectively. For the green PhOLEDs, device G2 obtained the highest device efficiency of CE, as high as  $48.0 \text{ cd A}^{-1}$  (PE of  $33.5 \text{ lm W}^{-1}$  and EQE of 9.2%). The reason is similar to that in the blue devices. In the red PhOLEDs, device R5, with the host FAF-SFX possessing the lowest HOMO/LUMO levels, achieved the highest device efficiency with a maximum CE of  $11.7 \text{ cd A}^{-1}$ , PE of  $11.6 \text{ lm/W}$  and EQE of 7.4%, and exhibited a much reduced efficiency roll-off. At luminances of 100 and  $1000 \text{ cd m}^{-2}$ , the CEs are still as high as  $11.6 \text{ cd A}^{-1}$  (EQE = 7.3%) and  $10.5 \text{ cd A}^{-1}$  (EQE = 6.2%), with efficiency roll-offs of 1.4% and 16.2%, respectively. This is due to the hole transport ability being higher than the electron transport ability in the red phosphor of  $\text{Ir}(\text{MDQ})_2(\text{-acac})$ ,<sup>21,22</sup> because some of the holes may directly inject into and transport on the HOMO level of  $\text{Ir}(\text{MDQ})_2(\text{acac})$  caused by the large hole injection barrier between the electron blocking layer and the host ( $>1.0 \text{ eV}$ ), and the large concentration of the phosphorescent emitters. FAF-SFX possesses the lowest-lying HOMO ( $-6.10 \text{ eV}$ ) and LUMO levels ( $-2.15 \text{ eV}$ ), which can best facilitate the electron injecting and hole blocking, and thus achieves better balanced carrier injection/transporting and higher device efficiency (Table 2).

Overall, among all these hosts, the DMOAF-SFX host achieves the best device performance in the RGB PhOLEDs and serves as the most efficient universal host. The maximum efficiencies of the blue, green, and red PhOLEDs are  $25.3$  (11.9%),  $48.0$  (9.2%),  $10.1$  (6.2%)  $\text{cd A}^{-1}$ , respectively. Based on host DMOAF-SFX, further application in a single-emitting-layer white PhOLED has been performed. The blue/yellow complementary single-emitting-layer white PhOLED (Device W) was fabricated, with the configuration of ITO/MoOx (2 nm)/*m*-MTDATA : MoOx (3 : 1) (15 nm)/*m*-MTDATA (20 nm)/Ir(ppz)<sub>3</sub> (10 nm)/DMOAF-SFX : Firpic:bis(4-phenylthieno[3,2-*c*]pyridinato-N,C2) acetylacetonate (Po-01) (10 wt%, 1 wt%, 10 nm)/

Bphen(40 nm)/LiF(1 nm)/Al(100 nm). Firpic and Po-01 were doped in the universal host DMOAF-SFX, serving as the single EML. Fig. 7a displays the normalized EL spectra of the WOLED at various voltages. Clearly, the emission from Po-01 slightly decreases with increasing driving voltage, which is possibly ascribed to the competition between electron trapping on the yellow-emitting chromophore sites and unperturbed charge through the organic layer.<sup>23,24</sup> The CIE coordinates are  $(0.275 \pm 0.015, 0.39 \pm 0.01)$  over a wide range of luminance ( $100\text{--}4932 \text{ cd m}^{-2}$ ), which shows good color stability (Fig. 7). The *J-V-L* characteristics and efficiency curves indicate that Device W exhibits a low onset voltage of 2.4 V with a maximum CE of  $18.8 \text{ cd A}^{-1}$ , PE of  $16.9 \text{ lm W}^{-1}$  and EQE of 7.6%.

## 4. Conclusions

In summary, we have developed a new, simple, two-step molecular design strategy to synthesize SFX/AF-based host materials by unconjugated connection of two separate functional segments of SFX and various AFs *via* very mild room temperature  $\text{MeSO}_3\text{H}$ -mediated Friedel-Crafts reaction. Multiple selective fine tuning of the FMO energy levels with constant high  $T_1$  has been achieved by either asymmetric substitution or electronegativity variation, which is regarded to be related to the unusual shift of the FMO charge distributions. This series of SFX/AFs hybrid compounds has been demonstrated to be utilized as universal hosts for low voltage multi-color RGB and white PhOLEDs. The multiple selective fine tuning of the electrical properties without interference of the  $T_1$  levels, can well explain the corresponding RGB PhOLEDs performances. This work provides good guidance for further rational design of more efficient SFX-based monochromic and universal RGB hosts by cumulative structural modifications.

## Acknowledgements

We express our sincere gratitude to the 973 projects (2012CB723402 and 2012CB933301), Priority Academic Program Development of Jiangsu Higher Education Institutions (PAPD) (YX03001), the National Natural Science Foundation of China (Grant nos 21373114, 61275033, and 21274064), National Natural Science Funds for Excellent Young Scholar (21322402), Doctoral Fund of Ministry of Education of China (20133223110007), Excellent science and technology innovation team of Jiangsu Higher Education Institutions (2013), and the Natural Science Foundation of Jiangsu Province (Grant nos BK2011761, 10KJB510013, and BM2012010) for their financial support.

## Notes and references

- M. A. Baldo, D. F. O'Brien, Y. You, A. Shoustikov, S. Sibley, M. E. Thompson and S. R. Forrest, *Nature*, 1998, **395**, 151–154.
- A. Kohler, J. S. Wilson and R. H. Friend, *Adv. Mater.*, 2002, **14**, 701–707.
- Y. Tao, C. Yang and J. Qin, *Chem. Soc. Rev.*, 2011, **40**, 2943–2970.

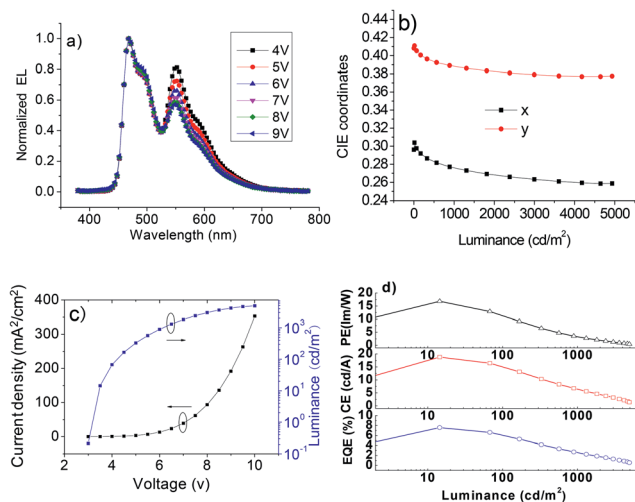


Fig. 7 The EL spectra (a) and CIE coordinates (b) at different operating voltages/luminance, the *J-V-L* characteristics (c) and efficiency curves (d) of the white device.

- 4 A. Chaskar, H.-F. Chen and K.-T. Wong, *Adv. Mater.*, 2011, **23**, 3876–3895.
- 5 H.-H. Chou and C.-H. Cheng, *Adv. Mater.*, 2010, **22**, 2468–2471.
- 6 S. J. Su, C. Cai and J. Kido, *Chem. Mater.*, 2011, **23**, 274–284.
- 7 S.-J. Su, C. Cai and J. Kido, *J. Mater. Chem.*, 2012, **22**, 3447–3456.
- 8 S. Gong, Y. Chen, J. Luo, C. Yang, C. Zhong, J. Qin and D. Ma, *Adv. Funct. Mater.*, 2011, **21**, 1168–1178.
- 9 S. Gong, Y. Chen, C. Yang, C. Zhong, J. Qin and D. Ma, *Adv. Mater.*, 2010, **22**, 5370–5373.
- 10 C. Cai, S.-J. Su, T. Chiba, H. Sasabe, Y.-J. Pu, K. Nakayama and J. Kido, *Org. Electron.*, 2011, **12**, 843–850.
- 11 W. Y. Hung, L. C. Chi, W. J. Chen, E. Mondal, S. H. Chou, K. T. Wong and Y. Chi, *J. Mater. Chem.*, 2011, **21**, 19249–19256.
- 12 H.-F. Chen, T.-C. Wang, S.-W. Lin, W.-Y. Hung, H.-C. Dai, H.-C. Chiu, K.-T. Wong, M.-H. Ho, T.-Y. Cho, C.-W. Chen and C.-C. Lee, *J. Mater. Chem.*, 2012, **22**, 15620–15627.
- 13 C.-L. Ho, L.-C. Chi, W.-Y. Hung, W.-J. Chen, Y.-C. Lin, H. Wu, E. Mondal, G.-J. Zhou, K.-T. Wong and W.-Y. Wong, *J. Mater. Chem.*, 2012, **22**, 215–224.
- 14 W.-Y. Hung, G.-M. Tu, S.-W. Chen and Y. Chi, *J. Mater. Chem.*, 2012, **22**, 5410–5418.
- 15 M.-S. Lin, L.-C. Chi, H.-W. Chang, Y.-H. Huang, K.-C. Tien, C.-C. Chen, C.-H. Chang, C.-C. Wu, A. Chaskar, S.-H. Chou, H.-C. Ting, K.-T. Wong, Y.-H. Liu and Y. Chi, *J. Mater. Chem.*, 2012, **22**, 870–876.
- 16 C. Han, Z. Zhang, H. Xu, J. Li, G. Xie, R. Chen, Y. Zhao and W. Huang, *Angew. Chem., Int. Ed.*, 2012, **51**, 10104–10108.
- 17 D. Yu, F. Zhao, C. Han, H. Xu, J. Li, Z. Zhang, Z. Deng, D. Ma and P. Yan, *Adv. Mater.*, 2012, **24**, 509–514.
- 18 L.-H. Xie, X.-Y. Hou, Y.-R. Hua, C. Tang, F. Liu, Q.-L. Fan and W. Huang, *Org. Lett.*, 2006, **8**, 3701–3704.
- 19 T.-L. Chiu and P.-Y. Lee, *Int. J. Mol. Sci.*, 2012, **13**, 7575–7585.
- 20 N. Matsusue, S. Ikame, Y. Suzuki and H. Naito, *J. Appl. Phys.*, 2005, **97**, 123512.
- 21 S. Reineke, F. Lindner, G. Schwartz, N. Seidler, K. Walzer, B. Luessem and K. Leo, *Nature*, 2009, **459**, 234–238.
- 22 W. S. Jeon, T. J. Park, S. Y. Kim, R. Pode, J. Jang and J. H. Kwon, *Org. Electron.*, 2009, **10**, 240–246.
- 23 M. C. Gather, R. Alle, H. Becker and K. Meerholz, *Adv. Mater.*, 2007, **19**, 4460–4465.
- 24 Q. Wang, J. Q. Ding, D. G. Ma, Y. X. Cheng, L. X. Wang, X. B. Jing and F. S. Wang, *Adv. Funct. Mater.*, 2009, **19**, 84–95.
- 25 L.-H. Xie, F. Liu, C. Tang, X.-Y. Hou, Y.-R. Hua, Q.-L. Fan and W. Huang, *Org. Lett.*, 2006, **8**, 2787–2790.
- 26 M. J. Frisch, G. W. Trucks, H. B. Schlegel, G. E. Scuseria, M. A. Robb, J. R. Cheeseman, G. Scalmani, V. Barone, B. Mennucci and G. A. Petersson, *et al.*, *Gaussian 09, Revision A.1*, Gaussian, Inc., Wallingford CT, 2009.